

Piezoelectric InGaAs/GaAs (111)B multiple quantum well photodiodes: optoelectronic properties by electron beam induced current and cathodoluminescence

M.J. Romero^{a,*}, D. Araújo^a, J.L. Sánchez-Rojas^b, E. Calleja^b, E. Muñoz^b, R. García^a

^aDepartamento de Ciencia de los Materiales e I.M. y Q.I., Facultad de Ciencias, Universidad de Cádiz, Apdo. 40, E-11510, Puerto Real (Cádiz), Spain

^bDepartamento de Ingeniería Electrónica, E.T.S.I. Telecomunicación. Universidad Politécnica de Madrid, Ciudad Universitaria s/n, E-28040 Madrid, Spain

Accepted 6 November 1998

Abstract

As a novel design parameter, the built-in piezoelectric field induced in InGaAs/GaAs (111)B heterostructures has potential applications in novel optoelectronic devices. Negative average field (NAF) and positive average field (PAF) p–i–n photodiodes are here studied by electron beam induced current (EBIC) and cathodoluminescence (CL). As a result of the negative potential envelope, carrier capture and recombination processes in the multiple quantum well (MQW) are shown to govern the carrier dynamic only in NAFs. Indeed, the electron beam induced current carriers become trapped at the potential minima located at the ends of the MQW giving rise to a long-range electric dipole. Using spatially resolved monochromatic cathodoluminescence measurements, a direct evidence of such long-range screening effect in (111) NAF diodes is given. © 1999 Elsevier Science Ltd. All rights reserved.

Keywords: Cathodoluminescence; Piezoelectric fields; Photodiodes

1. Introduction

The pseudomorphic InGaAs/GaAs heterostructures grown on high index GaAs substrates show a strain-induced piezoelectric field that is maximum for the $\langle 111 \rangle$ orientation. Applying the piezoelectric field as a design parameter, a novel band-engineering in piezoelectric (111)-oriented InGaAs/GaAs heterostructures has been demonstrated [1]. Indeed, in (111)B InGaAs/GaAs p–i–n structures with a multiple quantum well (MQW) embedded region, the average internal field in the MQW can be fitted to obtain device schemes with positive average fields (PAF) within the MQW, following the direction of the built-in field, or negative average fields (NAF), opposites to the built-in one (see inset of Fig. 1). In (111)PAF MQW diodes, as in (001) ones, the electrons photogenerated in the MQW are drifted towards the n-side, whereas the holes are drifted to the p-side. However, in (111)NAF photodiodes, because the field within the MQW is opposite to the built-in one, the excited carriers drift in the reverse sense and become trapped at the potential minima located at the ends of the active region, giving rise to an out-of-well screening effect of the field in

the MQW. This screening effect has been suggested to be the origin of the optical non-linearities in (111)NAF devices exploited in novel applications [2–4]. Previous photoluminescence analysis of such photodiode structures suggest a dipole formation [5]. This was definitively established by time-resolved photocurrent and optical-pump electrical-probe techniques [6].

In this work, a direct evidence of the out-of-well screening effect is reported from the cathodoluminescence (CL) technique that spatially resolves the different e-beam excited radiative transitions from the MQW of the (111)NAF diodes. The effect of different potential envelopes on the carrier transport is evaluated by electron beam induced current (EBIC). We illustrate the capability of the EBIC and CL techniques to simultaneously investigate electrical and optical properties with high spatial resolution.

2. Experimental details

Two diodes with identical structure but different Indium content, quantum well and barrier thickness were grown by MBE on (111)B n^+ GaAs substrates. Both heterostructures, detailed in Table 1, consist of $0.3 \mu\text{m } n^+$ GaAs (Si, $3 \times$

* Corresponding author.

E-mail address: manueljesus.romero@uca.es (M.J. Romero)

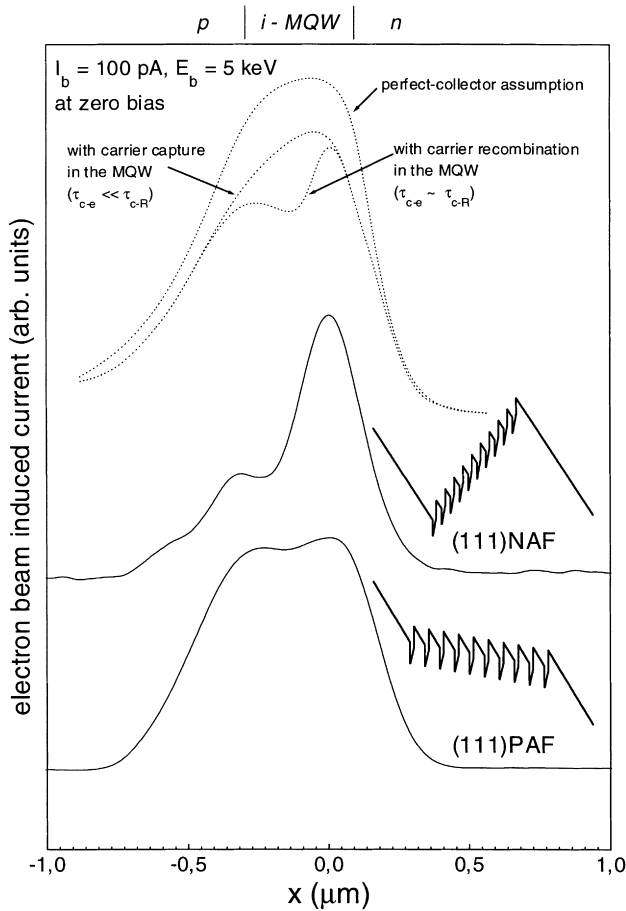


Fig. 1. EBIC linescans of the NAF and PAF InGaAs/GaAs(111)B pin MQW photodiodes at zero bias. The excitation level was $E_b = 5$ keV and $I_b = 100$ pA. The dashed lines are calculated linescans assuming the space-charge-region (SCR) as a perfect collector and taking into account the e-h capture and recombination processes in MQW. The inset shows the calculated conduction band potential profiles for both NAF and PAF diodes.

10^{18} cm^{-3}), a GaAs intrinsic region of $0.57 \mu\text{m}$ where 10 InGaAs/GaAs quantum wells are incorporated and $0.3 \mu\text{m}$ of p^+ GaAs ($\text{Be}, 2 \times 10^{18} \text{ cm}^{-3}$). The MQW of the PAF diode consist in 10 $\text{In}_{0.12}\text{Ga}_{0.88}\text{As}$ wells 100 \AA thick separated by GaAs barriers of 300 \AA thick. The MQW of the NAF diode consists of 10 $\text{In}_{0.17}\text{Ga}_{0.83}\text{As}$ wells 100 \AA thick

Table 1

InGaAs/GaAs(111)B MQW photodiode heterostructures. The differences between them are remarked

Material		Thickness (μm)		Carrier density (cm^{-3})	
PAF	NAF	PAF	NAF	PAF	NAF
	p^+ GaAs	300 nm		2×10^{18}	
	i GaAs	85 nm	160 nm	$ud (< 5 \times 10^{15})$	
i GaAs	i GaAs	300 \AA	150 \AA	$ud (< 5 \times 10^{15})$	
i $\text{In}_{0.12}\text{Ga}_{0.88}\text{As}$	i $\text{In}_{0.17}\text{Ga}_{0.83}\text{As}$ } $\times 10$	100 \AA	100 \AA	$ud (< 5 \times 10^{15})$	
	i GaAs	85 nm	160 nm	$ud (< 5 \times 10^{15})$	
	n^+ GaAs	300 nm		3×10^{18}	
	n^+ GaAs (substrate)	–		3×10^{18}	

with GaAs barriers of 150 \AA in thickness. The NAF and PAF labels are established at zero bias. Thus, applying different biases we modulate the average electric field. Indeed, above the threshold reverse bias the negative potential envelope becomes positive.

To carry out the EBIC and CL measurements, the photodiodes are mounted on an adapted holder in a JEOL-JSM820 scanning electron microscope in the normal-collector configuration, with the incident electron beam perpendicular to a freshly cleaved {110} face. The EBIC is measured using a head amplifier to a low input impedance amplifier (Matelect ISM-5A). The electron beam current is measured by a Faraday cup. The EBIC set-up allow us to apply a d.c. external bias voltage to the photodiode. The CL experiments are carried out at $T = 70 \text{ K}$ and electron beam energies (E_b) between 10 and 20 keV. The CL is collected using a semi-parabolic mirror adapted to an optical guide. A cryogenic CCD (Photometrics SDS9000) is attached to an Oriel 77400 Spectrograph / Monochromator for spectroscopic measurements. A CTI-Cryogenics 22C/350C helium closed-circuit cryostat attached to an anti-vibration system is used for low temperature measurements.

3. Results and discussion

Fig. 1 shows the spatial dependence of the EBIC across the MQW for both (111)PAF and (111)NAF diodes at zero bias. These linescans were recorded at $E_b = 5$ keV and $I_b = 100$ nA. Three regions can be distinguished:

1. First, in the p-side a decrease of the EBIC current is observed. This decrease is due to minority carrier (electron) diffusion to the depletion layer. Using a previously published method [7], we estimate an electron diffusion length of $L_e = 0.54 \mu\text{m}$ ($\pm 0.03 \mu\text{m}$) for the PAF diode and $L_e = 0.32 \mu\text{m}$ ($\pm 0.03 \mu\text{m}$) for the NAF diode. The surface recombination velocity is estimated to be $S/D \geq 10^6 \text{ cm}^{-1}$ (where D is the electron diffusion coefficient). These data are evaluated by comparison between EBIC calculations and experimental linescans. The model used for the calculations estimates first the spatial dependence of the electron–hole (e–h) generation [8,9] and is applied

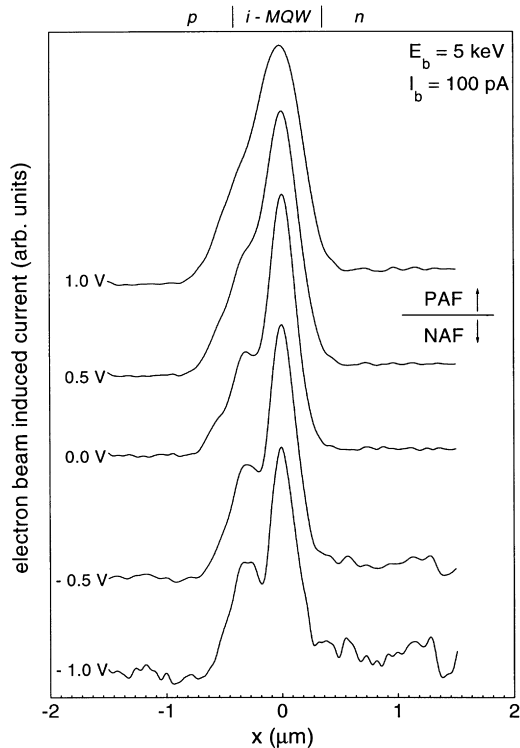


Fig. 2. EBIC linescans across the (111)NAF diode at different reverse biases. The transition from negative to positive average potential envelope (approximately at 0.7 V) is clearly evidence by the removal of the depression of the e-beam induced current in the MQW.

then for each differential volume of the continuity equation.

- Second, in the n-side a similar decrease of the EBIC current is observed. The minority carrier (hole) diffusion length is estimated to be $L_h = 0.25 \mu\text{m}$ ($\pm 0.03 \mu\text{m}$) and $L_h = 0.20 \mu\text{m}$ ($\pm 0.03 \mu\text{m}$) for PAF and NAF photodiodes, respectively, and a similar surface recombination velocity than in the p-side. These decreases (from PAF to NAF photodiodes) in the diffusion length are probably correlated with the introduction of lattice defects increasing the Indium fraction in the MQW.
- Finally, the third is the active region (MQW within the intrinsic region). The EBIC linescans across p–n junctions usually consist in a maximum at the depletion region with two decreases at each side governed by the minority carrier diffusion. Thus, the assumption of the space-charge-region (SCR) as a perfect collector can be made. However, a depression in the MQW of the EBIC across the (111)NAF diode is observed because the carrier capture and recombination processes govern the carrier dynamic in the MQW. In Fig. 1, the dashed lines are calculated linescans assuming the SCR as a perfect collector and when the e–h capture ($\tau_{c-e} \ll \tau_{c-R}$) and the e–h capture and recombination processes ($\tau_{c-e} \approx \tau_{c-R}$) govern the carrier kinetic in MQW. The latter affects the lateral distribution of the EBIC in two senses: (a) by increasing the e–h carrier capture rate in the MQW the

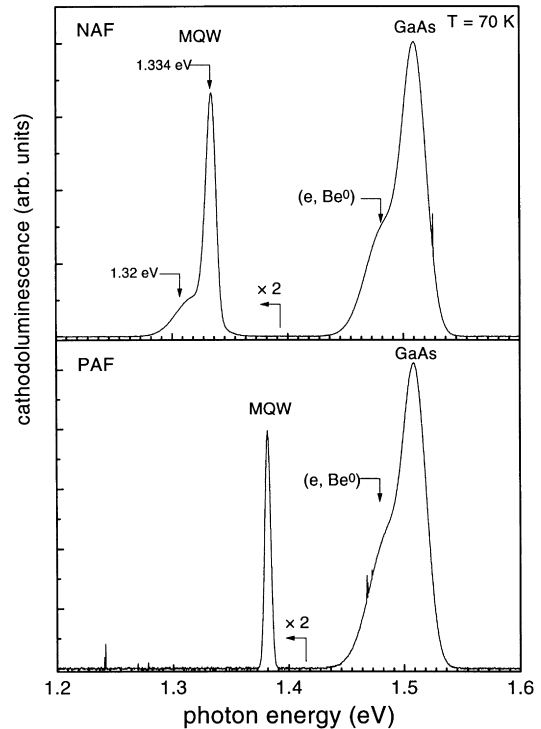


Fig. 3. CL spectra ($T = 70 \text{ K}$) of the NAF and PAF InGaAs/GaAs(111)B pin MQW photodiodes. They were recorded at $E_b = 10 \text{ keV}$ and $I_b = 3 \text{ nA}$ with a magnification of 35,000 centered in the junction.

extension of the EBIC lateral distribution decreases; (b) by increasing the e–h recombination rate, the depression of the EBIC response in the MQW enhances. Therefore, the latest shape of the EBIC depends of the relationship between the e–h capture, escape and recombination lifetimes.

A similar behavior is observed in the transition step by step from negative to positive potential envelopes applying a DC external bias voltage to the (111)NAF photodiode (Fig. 2). Below the threshold reverse bias (approximately at 0.7 V) the potential envelope remains negative. The capture processes govern the carrier dynamic in the MQW and a depression of the EBIC is experimentally observed. Above the threshold reverse bias the negative potential envelope becomes positive and the carrier dynamic is then governed by carrier escape. As a consequence, the depression at the MQW is removed.

The CL spectra ($T = 70 \text{ K}$) of the NAF and PAF MQW photodiodes are shown by Fig. 3. They were recorded at $E_b = 10 \text{ keV}$ and $I_b = 3 \text{ nA}$ with a magnification of 35,000 centered in the junction. The CL spectra are characterized by the GaAs e–h band-to-band transition and free-to-bound recombination related to Be acceptor (e, Be^0) and the luminescence of the InGaAs/GaAs MQW. For the NAF heterostructure, besides the intrinsic MQW luminescence at 1.334 eV, there is a non-resolved band approximately centered at 1.32 eV that has been previously reported to be related with a long-range screening effect in the active

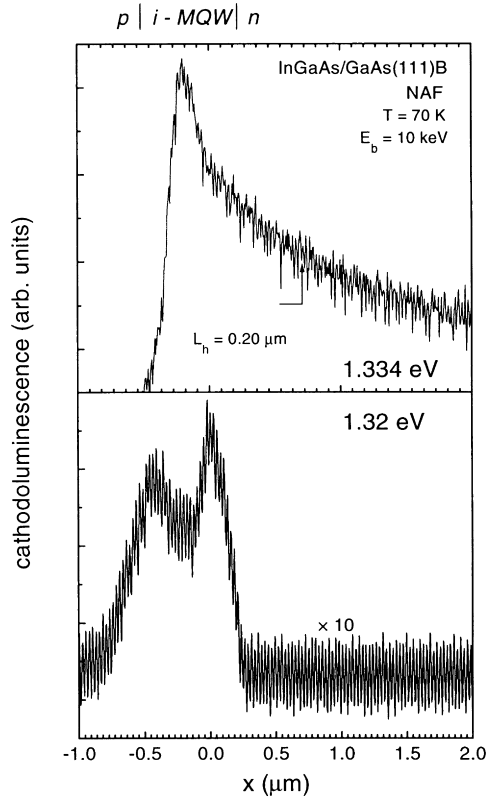


Fig. 4. Spatial distribution of the 1.334 eV and 1.32 eV MQW-related luminescences across the active region of the (111)NAF diode. The upper linescan was recorded with the 1.334 eV peak and the lower one was recorded with the low-energy band (approximately at 1.32 eV). The CL measurements were made on a freshly cleaved face perpendicularly to {111}.

region of the NAF InGaAs/GaAs (111)B photodiodes [1]. Here, we spatially resolve these emissions, as shown in the Fig. 4. The maximum emission for the 1.334 eV peak is localised at the center of the MQW. The exponential decay at the n-side is due to the diffusion of the minority carriers (holes) to the active region. Recording the linescan across the MQW with the 1.32 eV luminescence, the emission maximises at the edges of the MQW. The spatial dependence of this luminescence is a measure of the e-beam excited carrier accumulation, localised in the ends of the active region. These results are a direct evidence of the long-range screening effect in the MQW of the (111)NAF diode during the local e-beam excitation. The extension of the edge carrier accumulation induces an enlargement of the edge-QWs emission as their related energy levels vary from one to the other.

4. Computer simulation of the e-beam induced current

The computer simulation estimate the EBIC applying the continuity equations for different e-beam incidence coordinates across the active region of the diode. The current calculated is the addition of differential currents estimated

at each differential volume. The e–h collection efficiency of the (111) diodes and the shape of the EBIC across them are a result of the competition processes between the recombination in the QW, the QW capture and the QW escape. Thus, the 2D carrier density in the QW must be determined to estimate the rate of each process and is then introduced in the continuity equation. In summary, the sequence followed to estimate the theoretical EBIC current is the following: (i) from the Poisson equation, the band potential profile is estimated; (ii) the electron and heavy hole levels in the QWs are estimated from the Schrödinger equation considering the depletion as hundreds steps of flat potential, (iii) this allows the estimation of the two-dimensional carrier density in the wells and then the rates of radiative recombinations and capture–escape of carriers in the QWs. The generation of e–h, due to the e-beam excitation, is estimated at each differential volume by Monte Carlo calculations. The free parameters to be adjusted to fit with the experimental profile are the capture and radiative lifetime τ_{c-R} and the carrier capture–escape lifetime τ_{c-e} .

The competition between the different carrier lifetimes influences the continuity equation under the steady state conditions. For each differential volume we have:

$$\begin{aligned} \frac{\partial n}{\partial t} = G - R + \frac{1}{q} \nabla J = G - \sum_i \frac{n^i}{\tau_i} - n\mu \frac{\partial \mathcal{E}}{\partial x} + \mu \mathcal{E} \frac{\partial n}{\partial x} \\ + D \frac{\partial^2 n}{\partial x^2} = 0 \end{aligned} \quad (1)$$

In the QW Eq. (1) becomes:

$$\begin{aligned} G - R + \frac{1}{q} \nabla J = \int g(x, y, z) dV - \sum_i \frac{n^i}{\tau_i} + \frac{1}{q} \nabla J \\ = \int g(x, y, z) dV - \left[\frac{n^{\text{QW}}}{\tau_R} + \frac{n^{\text{QW}}}{\tau_{esc}} - \frac{nB}{\tau_{\cap}} \right] + \frac{1}{q} \nabla J \quad (2) \\ \int g(x, y, z) dV - \left[\frac{n^{\text{QW}}(x_k)}{\tau_{c-R}} - \frac{nB(x_{k+1})}{\tau_{c-e}} \right] + \frac{1}{q} \nabla J = 0 \end{aligned}$$

where k is the QW numeration. In the barriers we have:

$$\begin{aligned} G - R + \frac{1}{q} \nabla J = \int g(x, y, z) dV - \sum_i \frac{n^i}{\tau_i} + \frac{1}{q} \nabla J \\ = \int g(x, y, z) dV - \frac{nB}{\tau_{R,\text{bulk}}} + \frac{1}{q} \nabla J = 0 \end{aligned} \quad (3)$$

where G is determined by Monte Carlo simulations.

5. Conclusions

In conclusion, we illustrate the capability of EBIC and CL techniques to simultaneously investigate electrical and optical properties with high spatial resolution. From the EBIC

data, we access to the carrier dynamic in these piezoelectric structures modulated by the potential envelope of the active region. Indeed, for negative potential envelopes the capture and recombination processes govern the carrier dynamic whereas the capture–escape processes govern the positive ones. The CL measurements allow us to spatially resolve the radiative emissions from the MQW and a direct evidence of a long-range screening effect in NAF diodes is shown. The carrier accumulation effect is shown to enhance both the 1.334 and 1.32 eV peak FWHM due to the lateral extension of the carrier accumulation making little shift between the QW energy levels.

Acknowledgements

This work was supported by the CICYT (Comisión Interministerial de Ciencia y Tecnología) under MAT98-0823-CO3-02, CAM07T/0006/1997, and by the Junta de Andalucía through group TEP-0120.

References

- [1] J.L. Sánchez-Rojas, A. Sacedón, F. Calle, E. Calleja, E. Muñoz, *Appl. Phys. Lett.* 65 (17) (1994) 2214.
- [2] M. Livingstone, I. Galbraith, B.S. Wherrett, *Appl. Phys. Lett.* 65 (1994) 2271.
- [3] A.N. Cartwright, D.S. McCallum, T.F. Boggess, A.L. Smirl, T.S. Moise, L.J. Guido, R.C. Barker, B.S. Wherrett, *J. Appl. Phys.* 73 (1993) 7767.
- [4] J.F. Valtueña, I. Izpura, J.L. Sánchez-Rojas, E. Muñoz, E.A. Khoo, J.P.R. David, J. Woodhead, R. Grey, G.J. Rees, *Microelectronics J.* 28(8–10) (1997) 757.
- [5] V.L. Sánchez-Rojas, A. Sacedón, F. Cella, E. Calleja, E. Muñoz, *Phys. Rev. B* 53 (1996) 1546.
- [6] I. Izpura, J.F. Valtueña, J.L. Sánchez-Rojas, A. Sacedón, E. Calleja, E. Muñoz, *Solid State Electronics* 40(1–8) (1997) 463.
- [7] M.J. Romero, D. Araújo, J.D. Lambkin, R. García, *Mater. Sci. Engng B44* (1997) 57.
- [8] D. Araújo, J.-M. Bonard, J.-D. Ganière, F.-K. Reinhart, *Mater. Sci. Engng B24* (1994) 124.
- [9] J.-M. Bonard, D. Araujo, J.-D. Ganière, F.-K. Reinhart, *J. Appl. Phys.* 79 (1996) 8693.